An Ultrawideband Microfabricated Gold-Based Antenna Array for Terahertz Communications

Abdoalbaset Abohmra
University of Glasgow
Hasan Abbas
University of Glasgow
Jalil Kazim
University of Glasgow
Muhammad Rabbani
University of Birmingham
Chong Li
University of Glasgow
Akram Alomainy
Queen Mary University of London
Muhammad Imran
University of Glasgow
Qammer Abbasi (Qammer.Abbasi@glasgow.ac.uk)
University of Glasgow

Research Article

Keywords: wireless, Terahertz, bandwidth

Posted Date: November 30th, 2020

DOI: https://doi.org/10.21203/rs.3.rs-113085/v1

Version of Record: A version of this preprint was published at IEEE Antennas and Wireless Propagation Letters on January 1st, 2021. See the published version at https://doi.org/10.1109/LAWP.2021.3072562.

An Ultrawideband Microfabricated Gold-based Antenna Array for Terahertz Communications

Abdoalbaset Abohmra[1], Hasan T. Abbas[1], Jalil ur Rehman Kazim[1], Muhammad S. Rabbani[2], Chong Li[1], Akram Alomainy[3], Muhammad A. Imran[1], and Qammer H. Abbasi[1,*]

[1]James Watt School of Engineering, University of Glasgow, Glasgow, G12 8QQ, UK
[2]School of Electronic Electrical & System Engineering, University of Birmingham, Edgbaston B15 2TT, UK
[3]School of Electronic Engineering & Computer Science, Queen Mary University of London, London E1 4NS, UK
[*]Qammer.Abbasi@glasgow.ac.uk

ABSTRACT

The microwave frequency band typically used for wireless communications will soon become saturated and will no longer be able to fulfil the high bandwidth demands of modern communication networks. Terahertz (THz) communication has appeared as a highly attractive, future-generation wireless technology that offers higher spectral bandwidth and, therefore, higher data rates. However, the full exploitation of THz technologies is contingent upon the availability of energy efficient sources and devices. In this article, we presented a fabrication and measurement of microscale planar inverted cone antenna (PICA) array made of gold. Using an ungrounded coplanar waveguide feed, the microfabricated structure provides a bandwidth of 37.9 % with the resonant frequency of 0.925 THz. Given the cost of microfabrication is reducing substantially with rapid technological advancements, the results of this paper suggest that high-speed THz communications can be realised for widescale applications.

Introduction

The global average monthly mobile data consumption per device is expected to rise to 24 gigabytes in 2025[1] which will lead to great strains on the mobile networks. Terahertz (THz) communications has naturally been tagged as an attractive solution to the expected bandwidth crunch as THz networks have potential capacity in the range of several terabits per second[2–4]. However, the device technology to build sources and detectors is still in its infancy as compared to the established microwave and optical counterparts, that can not be merely scaled to THz frequencies owing to numerous reasons. THz technologies have been translated into various applications that spans biomedical science and engineering[5,6], imaging schemes[7,8], military[9], calibration systems for microwave sensors[10], space instrumentation[11], and environmental monitoring systems[12]. Most of the aforementioned applications particularly exploit the unique interactions of water molecules with the THz waves[13]. The so-called THz gap that ranges from 0.1 THz to 10 THz and this frequency range is less affected by the adverse climatic conditions like rain and fog[14]. However, with respective to the realisation of THz wireless systems, it remains a challenge to realise an ultrawideband, low-cost antenna that is scalable and easily integrated on-chip[15]. In this regard, a variety of THz nano-antenna designs that are scaled versions of the microwave frequency counterparts have been recently proposed that include printed dipoles[16–18], and simple patch antennas[19]. On-chip THz beamforming array systems that are fabricated on silicon have been also reported[20,21]. Surface plasmon enabled enhancement of the near-field further extends the promise of dipole- type antennas for THz communications[17]. Similarly, a nanoantenna array was also developed for subwavelength focusing of the THz waves[22]. A theoretical analysis of a highly directed antenna array having 16 elements at 0.3 THz was shown in[23] with a maximum directivity of 18.1 dBi. Despite these various attractive antenna designs, the patch antenna has the advantage of low cost, and relatively simple fabrication achieved through conventional semiconductor deposition techniques[24].

At THz frequencies, the substrate thickness inevitably becomes comparable to the wavelength[25], which prevents the efficient design of the planar antenna feeding networks, due to the change in the impedance. The ungrounded coplanar waveguide (UCPW) feed is a viable solution to provide not only just good impedance matching with a sufficient substrate thickness, but low transmission loss, small frequency dispersion, and most importantly easy integration with the monolithic circuit designs. In addition to this, the handling of the antenna during the fabrication also becomes safer as no extra processing measures are required for the back layer of the substrate[26].

Amongst the antenna designs that yield an ultrawideband (UWB) response with an omnidirectional spatial coverage, the planar inverted cone antenna (PICA) has emerged as one of the most promising designs in the last two decades. A PICA is composed of a semicircle, which is extended into an inverted cone from the flat side. Performance-wise, the PICA is known to produce an impedance bandwidth of 20:1 at microwave frequencies[27,28]. Moreover, due to the flat profile, the PICA exhibits

mechanical stability due to which it is increasingly being used for commercial applications that require high bandwidth in an omnidirectional way. In this paper, we presented for the first time in literature a fabricated and experimentally measured, novel and simple ultrawideband, omnidirectional 1×4 THz PICA array with a 37.9 % bandwidth with a central frequency of 0.92 THz. The simple profile of the antenna array and excellent radiation characteristics can pave the way for realising truly UWB wireless communications in the THz frequency band.

Results

Antenna Design

The proposed antenna design was simulated and analysed using a three-dimensional, full-wave commercial electromagnetics solver, Dassault Systemes CST Studio Suite 2019. An array of gold-based PICAs was designed at 1 THz on a silicon substrate, having a dielectric constant, $\varepsilon_r = 11.9$ and thickness, $h = 600$um. The feed line dimensions, L, and W were calculated using standard microstrip transmission line based expression to obtain a characteristic impedance of 50Ω. A conventional T-divider circuit approach was used for the feeding line design so that each antenna element is excited uniformly. The feed line widths, W_f^n required to obtain 50, 70, and 100 Ω characteristic impedance at various junctions is obtained using,

$$W_f^n = 7.48h \exp\left(-Z_0^n \frac{\sqrt{\varepsilon_r + 1.41}}{87}\right) - 1.25t, \tag{1}$$

Z_0^n is the characteristic impedance of the n^{th} junction, and t is the trace thickness. Similarly, the length L of the feed line can be calculated using, $L_t = (2M+1) \times \lambda$. where M is an integer and λ is the wavelength[29]. The obtained values were further optimised using 'trust region' algorithm available in the CST Studio Suite solver. The designed antenna structure along with the feeding network is shown in Fig. 1. Furthermore, the dimensions of the antenna and the feeding lines are described in Table 1.

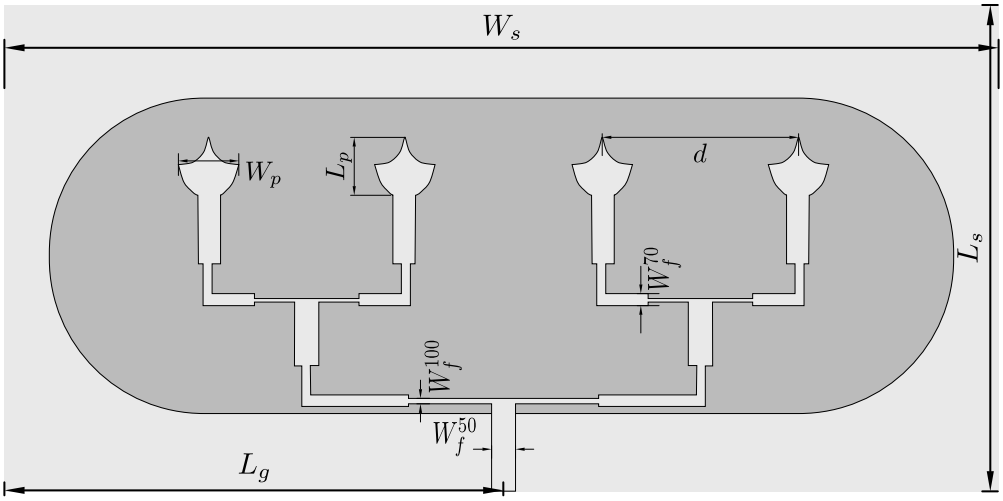

Figure 1. The geometry and dimensions the PICA array and the feeding network.

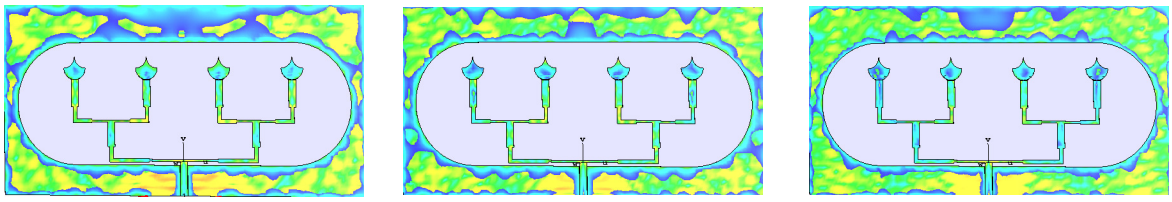

Figure 2. Visualisations of the electric field distribution at (a) 0.75 THz, (b) 0.925 THz, and (c) 1.10 THz.

Figure 2 shows the surface electric current distribution of the PICA at three different operating frequencies, namely 0.75THz, 0.925THz, and 1.10THz respectively, and these results show that the current reaches the tip of the PICA, causing radiation of the EM waves. At 0.75 THz, the surface electric current is strongly excited on the top surface of the gold metallic posts,

Dimensions	Description	Value (μm)
g	CPW feeding gap	1
L_p	Patch Length	100
W_p	Patch width	120
W_s	Substrate width	1000
L_s	Substrate length	2000
h	Substrate thickness	600
W_f^{50}	50Ω feed line width	45
W_f^{70}	70Ω feed line width	20
W_f^{100}	100Ω feed line width	9.9
d	Spacing between Antenna elements	300
L_g	Ground plane length	978

Table 1. The dimensions of the gold PICA array.

whereas the current on the four side tips also contributes to the radiation of the antenna, though its magnitude is much smaller than the counterpart on the metallic posts. Besides, the electric field over the edges of the radiating aperture is also strongly excited.

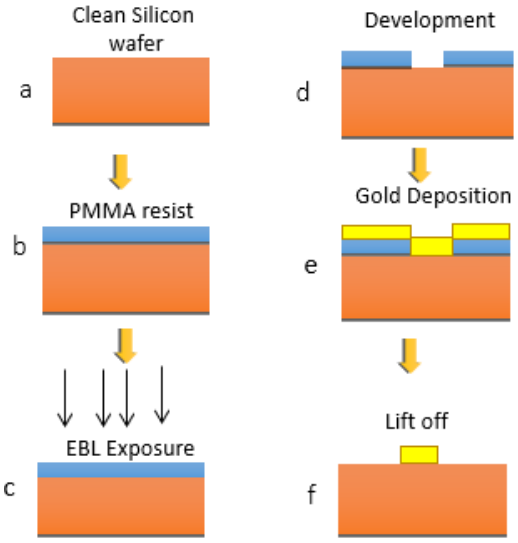

Figure 3. Fabrication process flow based on E-beam Lithography

In order to make the antenna resistant to corrosion and chemically stable, we chose gold as the radiating material. In addition, at THz frequencies, gold exhibits a high electrical conductivity with a lower skin depth ($\sim$ 80 nm at 1 THz)[30]. It is easily deposited using traditional deposition techniques such as sputtering, evaporation, and electroplating with a high melting point[31]. For the fabrication of sub-micron structures, electron beam lithography (EBL) is utilised to transfer the pattern onto a resist layer that is pre-coated on the surface of a wafer. In general, a shorter wavelength is key to achieve smaller feature sizes. With EBL nano scale THz antenna designs can be realised.

Antenna Fabrication

The fabrication process of the proposed 1×4 PICA array was carried out at the James Watt Nanofabrication Centre (JWNC) at the University of Glasgow. The four-step fabrication process is illustrated in in Fig. 3, where the sample undergoes cleaning, after which the photoresist is spun on the wafer. After that, the design is transferred using the EBL and the last step involves the metal liftoff. The execution of these steps initially involved a polymethyl methacrylate (PMMA) resist which was spin-coated onto the silicon substrate with a thickness of 1.2μm. The higher sensitivity photoresist requires a lower dose which ultimately determines the exposure times. The exposure dose from the e-beam source was tested on the PMMA photoresist before the process of fabrication and it was found that $650\mu\text{m}/\text{cm}^2$ dose was optimum to obtain a good resolution. A 2.5:1 developer was

used to develop the PMMA for 30 s and rinsed afterwards with isopropyl alcohol for 20 s. Lastly, a 500 nm layer of gold was deposited on the developed wafer. The unwanted gold was removed by dissolving the resist in acetone solution for 4 hours. The size and geometry of the obtained fabricated structure can be ascertained from Fig. 4, which also contains images recorded from an ultrahigh resolution field emission scanning electron microscope (FESEM), SU8240 by Hitachi High-Technologies.

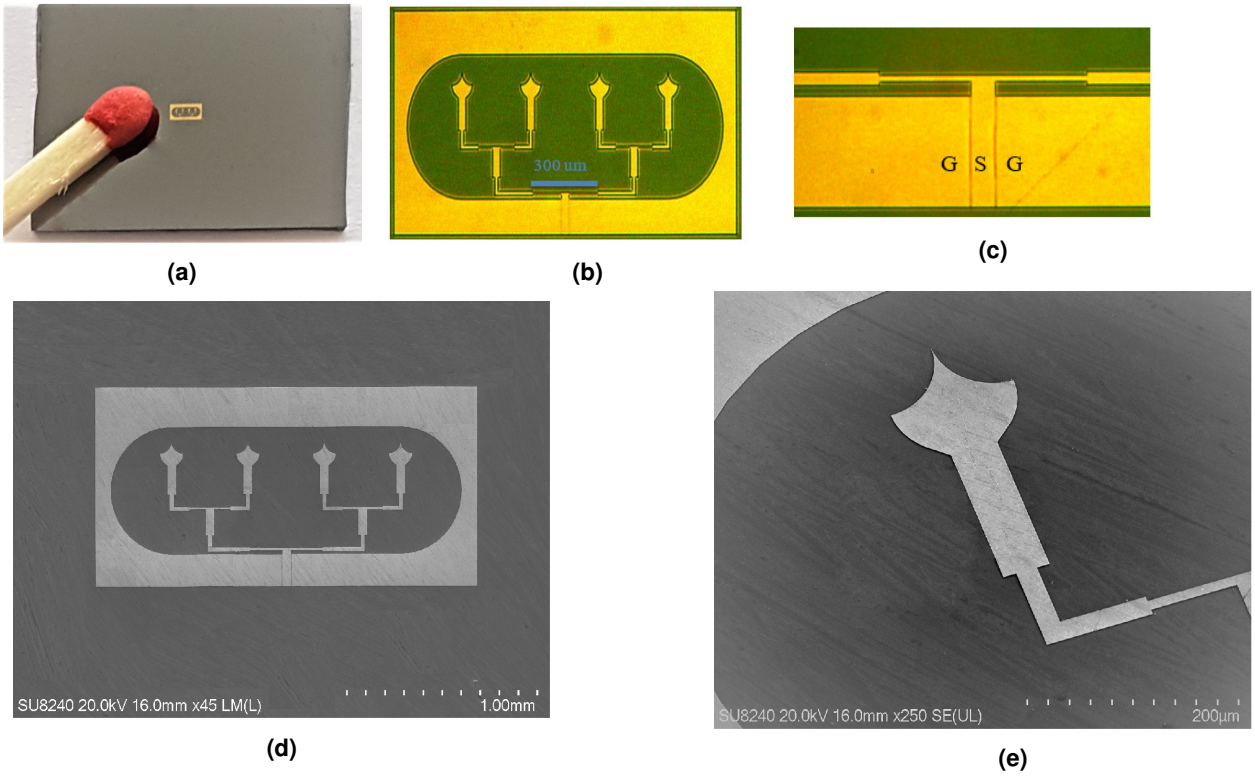

Figure 4. (a) Comparison of the size of the fabricated 1×4 PICA array with a matchstick. Photomicrographs of: (b) the array structure and, (c) the ungrounded CPW feeding network. High-resolution images obtained using a FESEM of: (d) Array structure and, (e) feeding transmission line for a PICA element of the array.

Measurement

As per the authors' knowledge, the fabricated on-chip antenna was measured in the THz frequency band, for the first time in literature, where we used a Cascade Microtech THz wave vector network analyser (VNA) coupled with a Virginia Diodes Inc. VNA extender to obtain the scattering properties of the PICA array in the $0.75 - 1.10$THz frequency range. The VNA was connected with a separate set of sub-millimetre scale THz wave probes that provided an on-wafer ground-signal-ground (G-S-G) electrical contact for the measurement in the desired frequency range of $0.75 - 1.10$THz. The G-S-G probe having a pitch of 25μm was carefully placed on the ungrounded CPW feeding line of the proposed antenna for measurement. Figure 5a shows the electric and magnetic field distribution around the CPW line, whereas Fig. 5b illustrates how the THz probe was used to excite the ungrounded CPW feed line.

The complete measurement setup is illustrated in Fig. 6, which was configured at the Metamaterials Engineering Laboratory at the University of Birmingham. The THz probe used offers a low insertion loss, i.e., < 1.5dB with good sample visibility. The VNA was calibrated for 1-port S-parameter measurement using the short-open-load-thru (SOLT) calibration process on a cascade impedance substrate standard. The simulated and measured reflection coefficients of the 1×4 PICA array are shown in Fig. 7, which shows the excellent antenna performance as the whole response is below the 10dB range. Moreover, both the measurement and simulation results exhibit good agreement with each other, and the disparity is attributed to the unpredictable reflection from the surroundings of the experimental setup. In addition, the antenna was fabricated on a carrier wafer which was kept larger than the simulated substrate to ensure convenient handling of the fabricated antenna, resulting in a slight impedance mismatch with the feeding network. This can be observed by a series of ripples that can be seen in the measured scattering response. Figure 8 shows the simulated antenna performance in terms of the antenna radiation efficiency and the gain achieved by the array in the operating frequency range. It can be seen that the gain of the antenna is maintained above 70%. Although, this is lower as compared to antenna designs at microwave frequencies where the radiating element acts nearly as a perfect

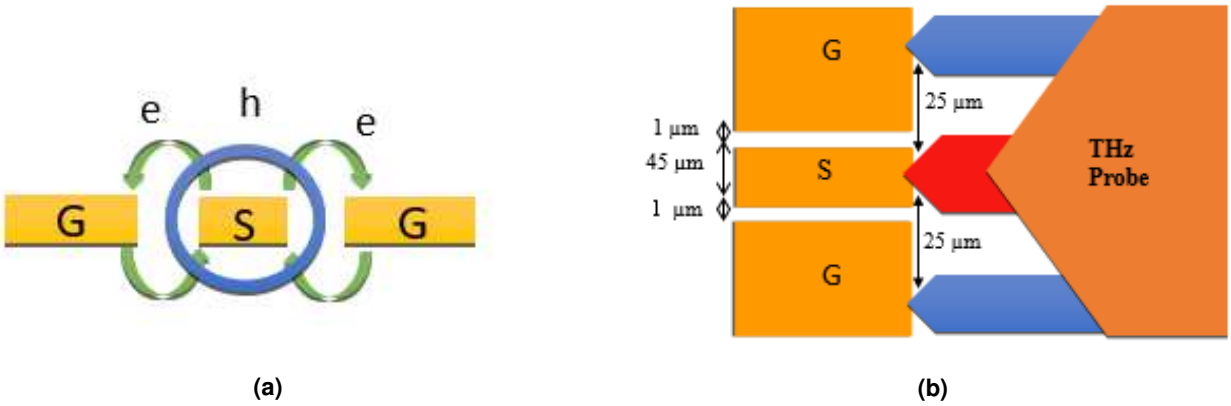

(a) (b)

Figure 5. The ungrounded CPW feeding network. (a) Illustration of the electric and magnetic field distributions around the ungrounded CPW and, (b) schematic of the probe measurement contact with the central signal transmission line (S) and ground plane (G).

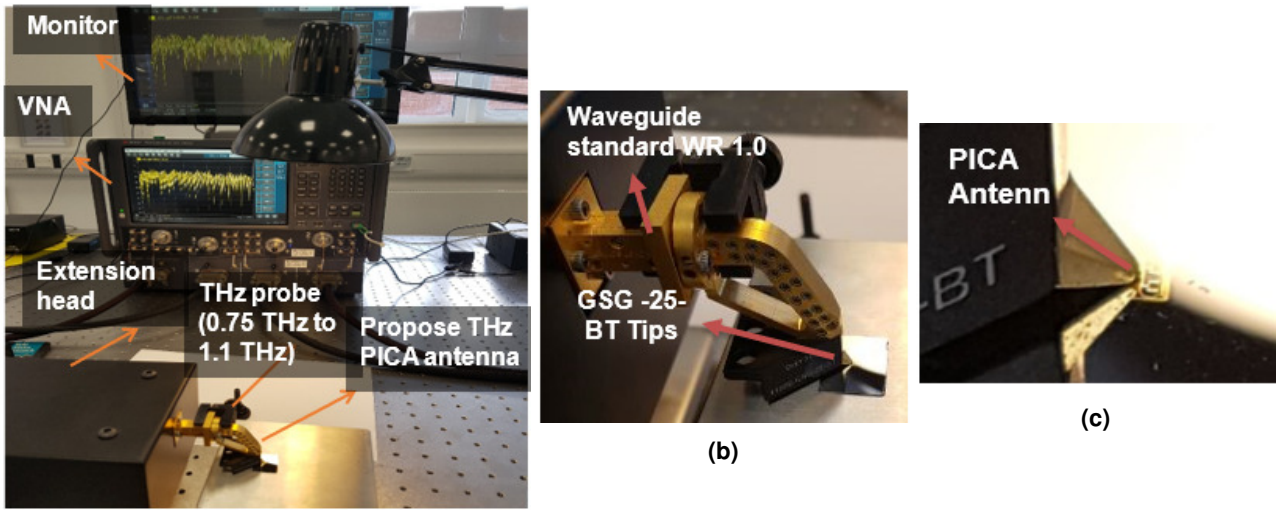

(a) (b) (c)

Figure 6. The experimental setup used to measure the scattering parameters. (a) Eye-view of the setup, (b) a GSG-25-BT THz probe (0.75 - 1.10 THz) contact location and, (c) placement of the probe on the PICA.

electric conductor, the conductivity of gold at THz frequencies is complex valued where the imaginary part contributes to losses. Further investigations in which a substrate with a lower dielectric constant is used, can improve the radiation efficiency of the designed antenna. Other performance parameters such as the antenna gain and directivity are shown in Fig. 8b, which indicates a high realised realised gain in the range of 12.5 – 16 dBi.

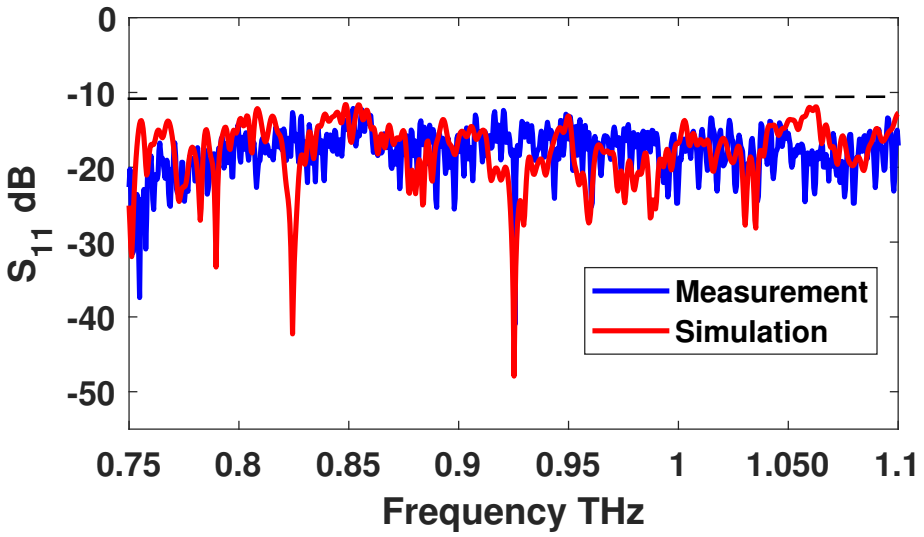

Figure 7. Measured and simulated reflection coefficient of the 1×4 PICA array array.

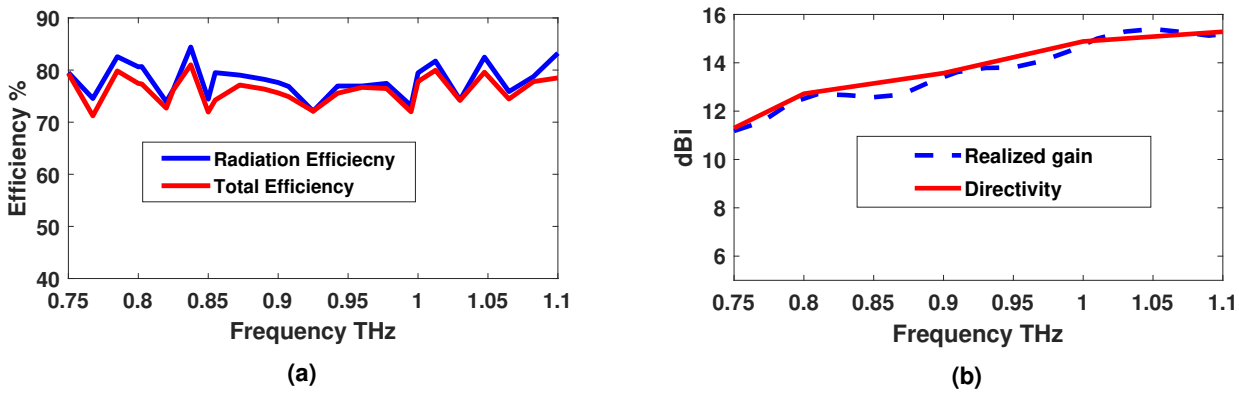

Figure 8. Simulated results of the 1×4 PICA array, where (a) the radiation and total efficiency is shown and in, (b) the realised gain.

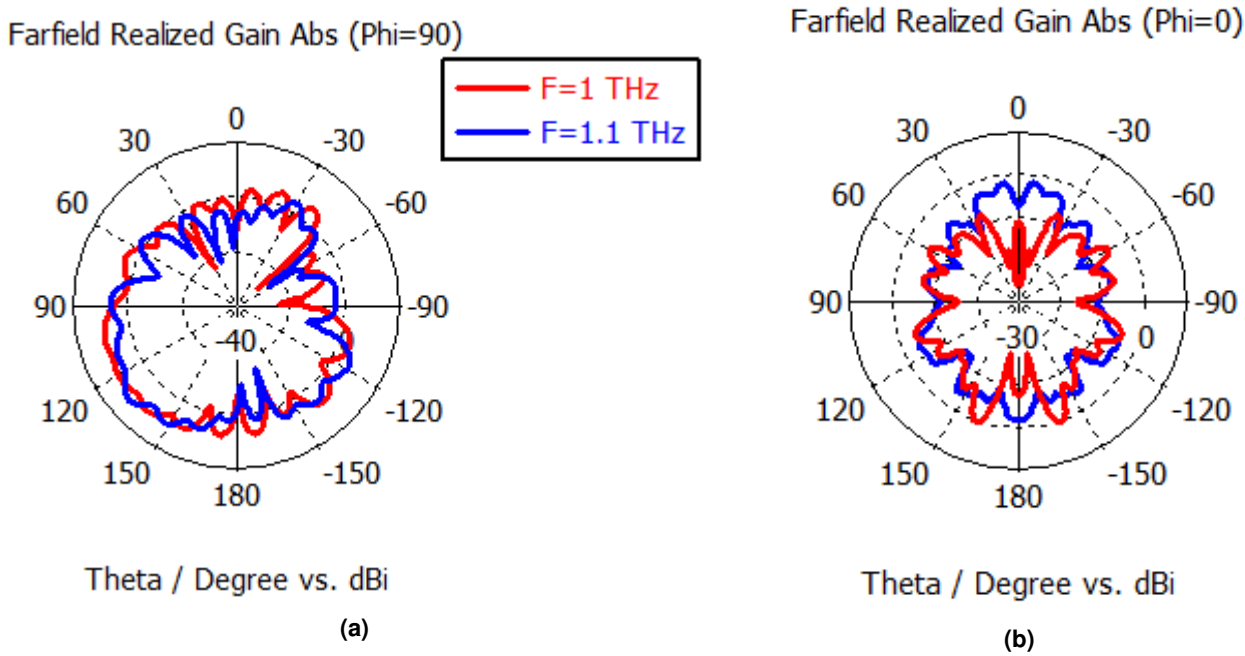

Figure 10. Simulated radiation pattern of the proposed antenna element at different frequencies throughout the operating band. f = 1.0 THz, and f = 1.10 THz

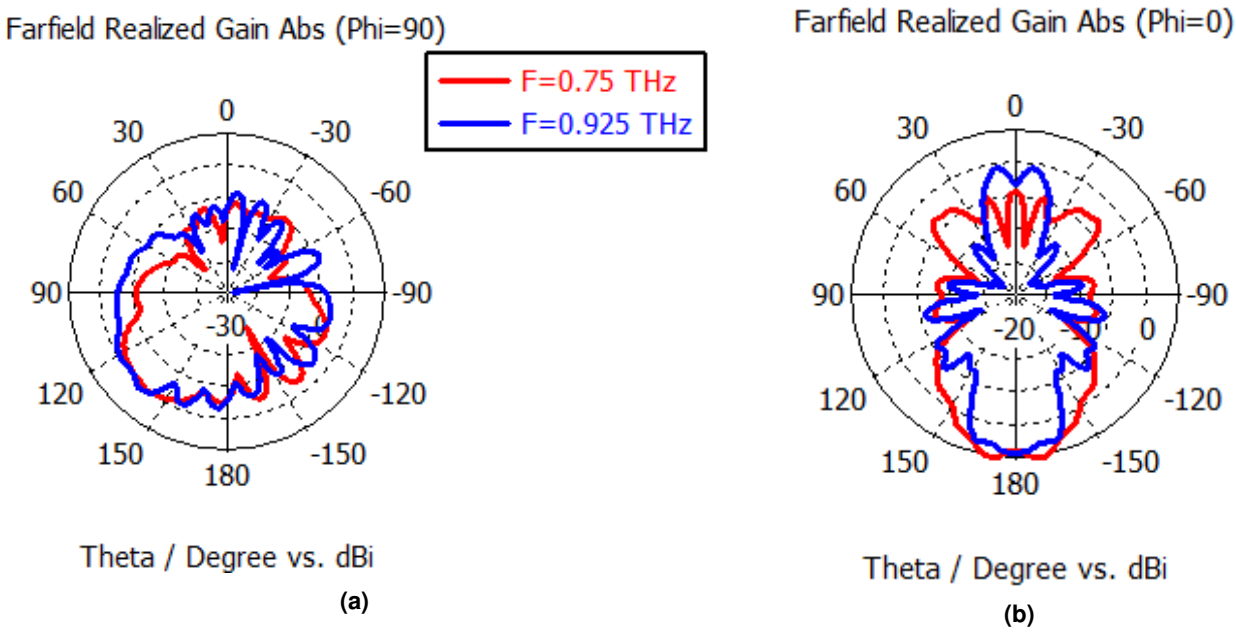

Figure 9. Simulated radiation pattern of the proposed antenna element at two frequencies, 0.75 THz, and 0.925 THz.

Figures 9 and 10 present the simulated radiation patterns of the designed antenna array at 0.75 THz, 0.925 THz, and at 1 THz and 1.10 THz respectively. The radiation patterns are presented at E− and H− planes. Due to the large dielectric constant of the silicon substrate, most of the radiation is directed towards the substrate. This is a common problem with antennas fabricated on high dielectric constant substrates, which at THz frequencies is often circumvented by using a hemispherical lens. The sidelobe level is increased and the maximum sidelobe is observed at 1.10 THz. Therefore, the ripples in the radiation pattern may lead to a degradation in the antenna performance which is mainly caused by metal loss and skin depth effect. In Figs. 9 and 10, the radiation patterns show high main lobe magnitudes along with lower backlobe levels.

1 Conclusion

In this letter, we designed and fabricated a gold-based 1×4 planar inverted cone antenna array operating in the terahertz (THz) frequency range of 0.75 - 1.10 THz. We used simple and commonly available metal deposition techniques to fabricate the structure. An ungrounded coplanar waveguide feeding line was used to excite the antenna. As per our knowledge, the proposed design is a first instance of THz antenna for which the scattering response was measured. Our design achieved a measured -10 dB impedance bandwidth of 400 GHz at the centre frequency of 0.925 THz. Results also show that other antenna performance characteristics such as radiation efficiency and gain are also high. We anticipate the designs and techniques used in this letter can launch a new research direction for realising THz frequency ultrawideband antennas for enabling high speed wireless communications in future.

References

1. Cerwall, P. *et al.* Ericsson mobility report - june 2020. Tech. Rep., Ericsson, SE-164 80 Stockholm, Sweden (2020).
2. Koch, M. Terahertz communications: A 2020 vision. In *Terahertz frequency detection and identification of materials and objects*, 325–338 (Springer, 2007).
3. Laskar, J. *et al.* The next wireless wave is a millimeter wave. *Microw. J.* **50**, 22 (2007). Publisher: Citeseer.
4. Jornet, J. M. & Akyildiz, I. F. Graphene-based Plasmonic Nano-Antenna for Terahertz Band Communication in Nanonetworks. *IEEE J. on Sel. Areas Commun.* **31**, 685–694, DOI: 10.1109/JSAC.2013.SUP2.1213001 (2013).
5. Siegel, P. H. Terahertz technology in biology and medicine. *IEEE transactions on microwave theory techniques* **52**, 2438–2447 (2004). Publisher: IEEE.
6. Fitzgerald, A. J. *et al.* An introduction to medical imaging with coherent terahertz frequency radiation. *Phys. Medicine & Biol.* **47**, R67 (2002). Publisher: IOP Publishing.

7. Choi, M. K., Taylor, K., Bettermann, A. & Van der Weide, D. W. Broadband 10–300 GHz stimulus-response sensing for chemical and biological entities. *Phys. Medicine & Biol.* **47**, 3777 (2002). Publisher: IOP Publishing.

8. Kim, G.-J., Han, W.-K., Kim, J.-I. & Jeon, S.-G. High resolution terahertz imaging (T-ray) with a horn antenna. In *35th International Conference on Infrared, Millimeter, and Terahertz Waves*, 1–2 (IEEE, 2010).

9. Woolard, D. L., Jensen, J. O. & Hwu, R. J. *Terahertz science and technology for military and security applications*, vol. 46 (world scientific, 2007).

10. Cofield, R. E. & Stek, P. C. Design and field-of-view calibration of 114-660-GHz optics of the Earth observing system microwave limb sounder. *IEEE transactions on geoscience remote sensing* **44**, 1166–1181 (2006). Publisher: IEEE.

11. Siegel, P. H. THz instruments for space. *IEEE Transactions on Antennas Propag.* **55**, 2957–2965 (2007). Publisher: IEEE.

12. Tonouchi, M. Cutting-edge terahertz technology. *Nat. photonics* **1**, 97–105 (2007). Publisher: Nature Publishing Group.

13. Woolard, D. L., Brown, R., Pepper, M. & Kemp, M. Terahertz frequency sensing and imaging: A time of reckoning future applications? *Proc. IEEE* **93**, 1722–1743 (2005). Publisher: IEEE.

14. Williams, G. P. Filling the THz gap—high power sources and applications. *Reports on Prog. Phys.* **69**, 301 (2005). Publisher: IOP Publishing.

15. Luk, K.-M. *et al.* A microfabricated low-profile wideband antenna array for terahertz communications. *Sci. reports* **7**, 1–11 (2017). Publisher: Nature Publishing Group.

16. Lee, D.-K. *et al.* Highly sensitive and selective sugar detection by terahertz nano-antennas. *Sci. reports* **5**, 1–7 (2015). Publisher: Nature Publishing Group.

17. Razzari, L. *et al.* Terahertz dipole nanoantenna arrays: resonance characteristics. *Plasmonics* **8**, 133–138 (2013). Publisher: Springer.

18. Gray, D., Lu, J. W. & Thiel, D. V. Electronically steerable Yagi-Uda microstrip patch antenna array. *IEEE Transactions on antennas propagation* **46**, 605–608 (1998). Publisher: IEEE.

19. Feuillet-Palma, C., Todorov, Y., Vasanelli, A. & Sirtori, C. Strong near field enhancement in THz nano-antenna arrays. *Sci. reports* **3**, 1–8 (2013). Publisher: Nature Publishing Group.

20. Sengupta, K. & Hajimiri, A. A 0.28 THz power-generation and beam-steering array in CMOS based on distributed active radiators. *IEEE J. Solid-State Circuits* **47**, 3013–3031 (2012). Publisher: IEEE.

21. Caster II, F. *et al.* Design and analysis of a W-band 9-element imaging array receiver using spatial-overlapping super-pixels in silicon. *IEEE J. Solid-State Circuits* **49**, 1317–1332 (2014). Publisher: IEEE.

22. Feuillet-Palma, C., Todorov, Y., Vasanelli, A. & Sirtori, C. Strong near field enhancement in THz nano-antenna arrays. *Sci. reports* **3**, 1–8 (2013). Publisher: Nature Publishing Group.

23. Sengupta, K. & Hajimiri, A. A 0.28 THz power-generation and beam-steering array in CMOS based on distributed active radiators. *IEEE J. Solid-State Circuits* **47**, 3013–3031 (2012). Publisher: IEEE.

24. Luk, K.-M. *et al.* A microfabricated low-profile wideband antenna array for terahertz communications. *Sci. reports* **7**, 1–11 (2017). Publisher: Nature Publishing Group.

25. Brown, E., Lee, A., Navi, B. & Bjarnason, J. Characterization of a planar self-complementary square-spiral antenna in the thz region. *Microw. optical technology letters* **48**, 524–529 (2006).

26. Hincapie, R. & Sierra, J. E. *Advanced Transmission Techniques in WiMAX* (BoD–Books on Demand, 2012).

27. Suh, S.-Y., Stutzman, W. L. & Davis, W. A. A new ultrawideband printed monopole antenna: The planar inverted cone antenna (pica). *IEEE Transactions on Antennas Propag.* **52**, 1361–1364 (2004).

28. Suh, S.-Y., Stutzman, W., Davis, W., Waltho, A. & Schiffer, J. A novel cpw-fed disc antenna. In *IEEE Antennas and Propagation Society Symposium, 2004.*, vol. 3, 2919–2922 (IEEE, 2004).

29. Balanis, C. A. *Antenna theory: analysis and design* (John wiley & sons, 2016).

30. Walther, M. *et al.* Terahertz conductivity of thin gold films at the metal-insulator percolation transition. *Phys. Rev. B* **76**, 125408 (2007).

31. Kabashin, A. V. *et al.* Nanofabrication with pulsed lasers. *Nanoscale research letters* **5**, 454 (2010).

Acknowledgements

This work is supported in part by the Engineering and Physical Sciences Research Council (EPSRC) under grant number: EP/R511705/1. A. A. would like to thank the Government of Libya for funding his doctoral studies.

Author Contributions

A. A. proposed the method, wrote the manuscript, and performed the simulations. H. A. planned the writing and proposed the antenna design J. K. assisted in fabricating the structure. M. R. organised the antenna measurement. C. L. obtained the SEM images and discussed the results. A. A. contributed in the review and the simulations. M. I. analysed the results. Q. A. supervised and managed the project and co-wrote the manuscript. All the authors reviewed the results and contributed to reviewing the manuscript.

Figures

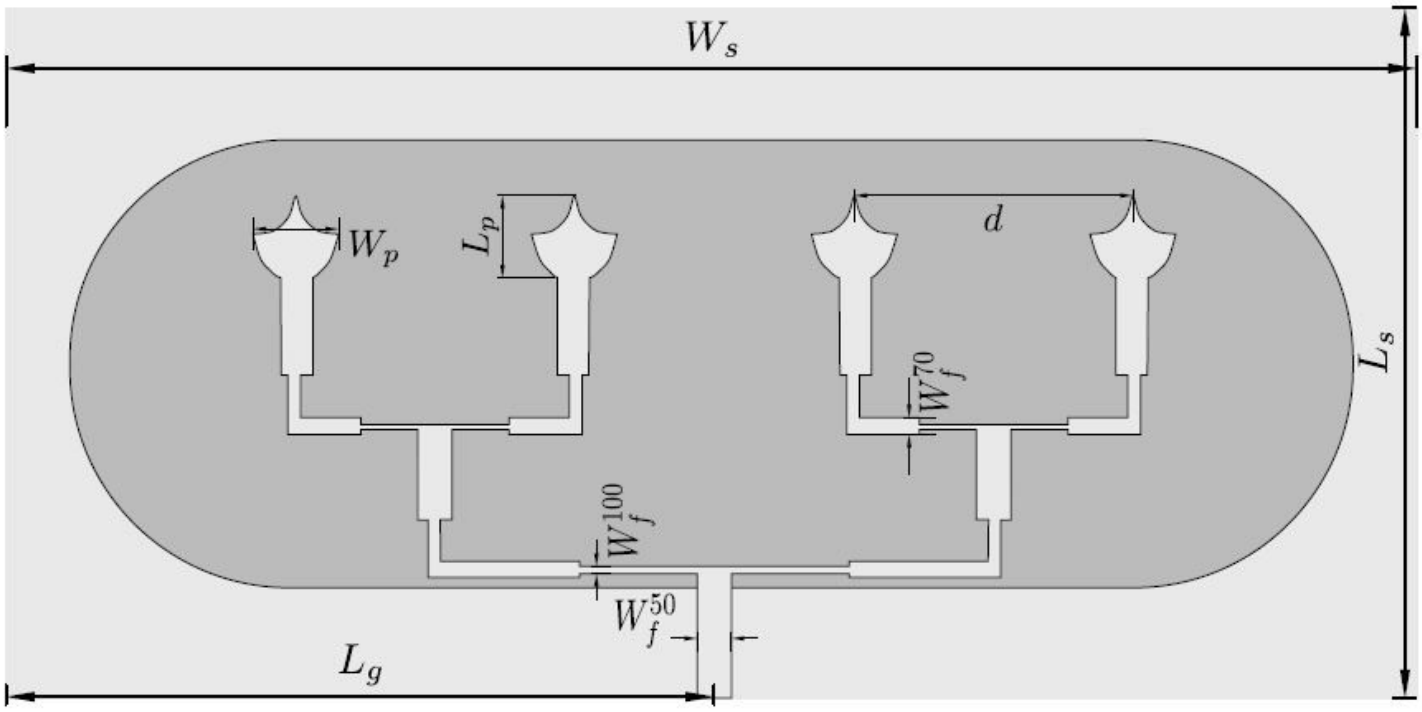

Figure 1

The geometry and dimensions the PICA array and the feeding network.

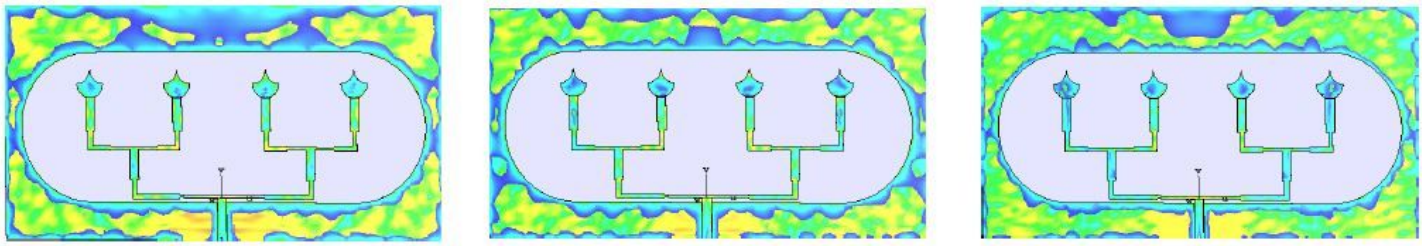

Figure 2

Visualisations of the electric field distribution at (a) 0.75 THz, (b) 0.925 THz, and (c) 1.10 THz.

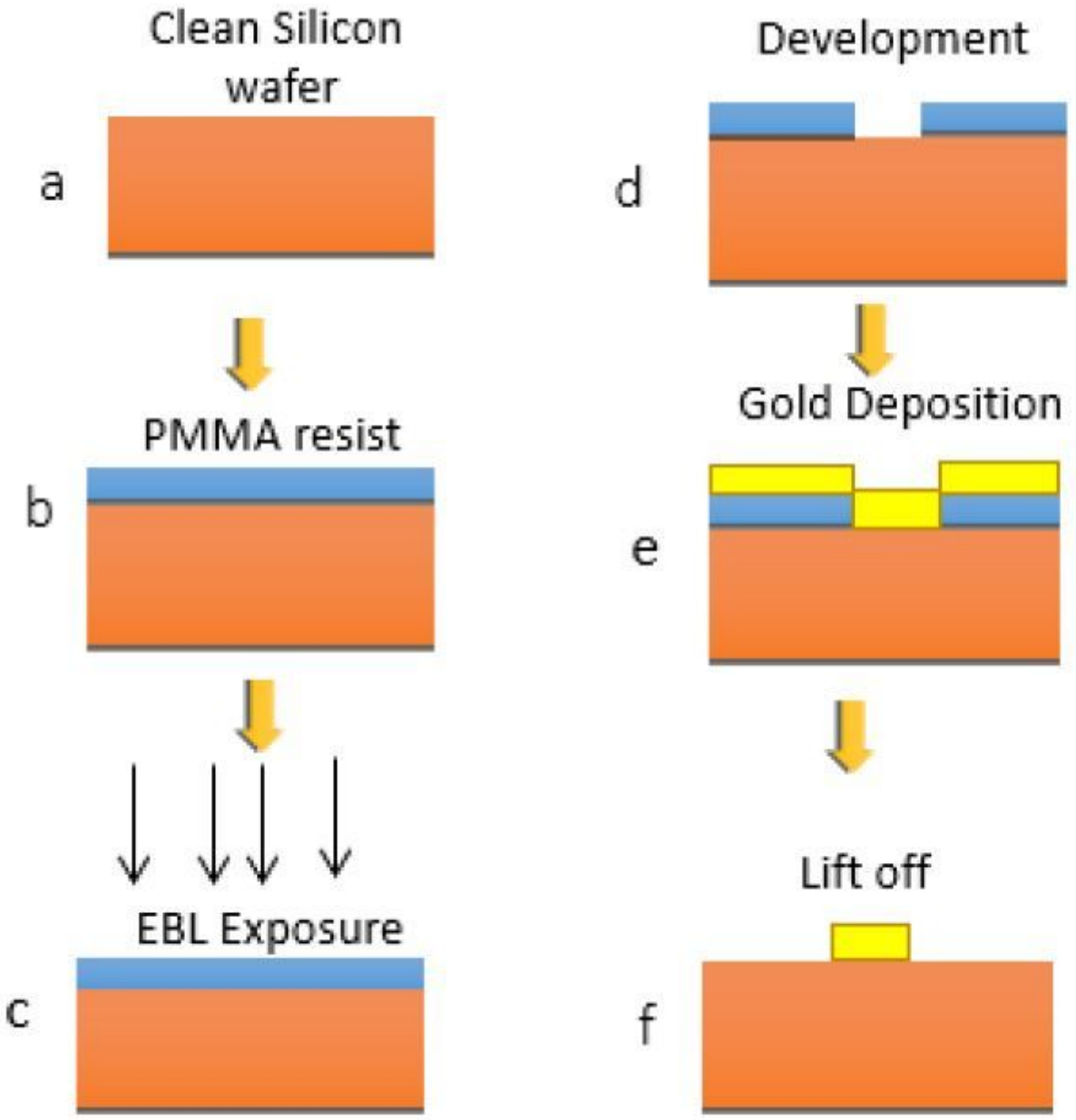

Figure 3

Fabrication process flow based on E-beam Lithography

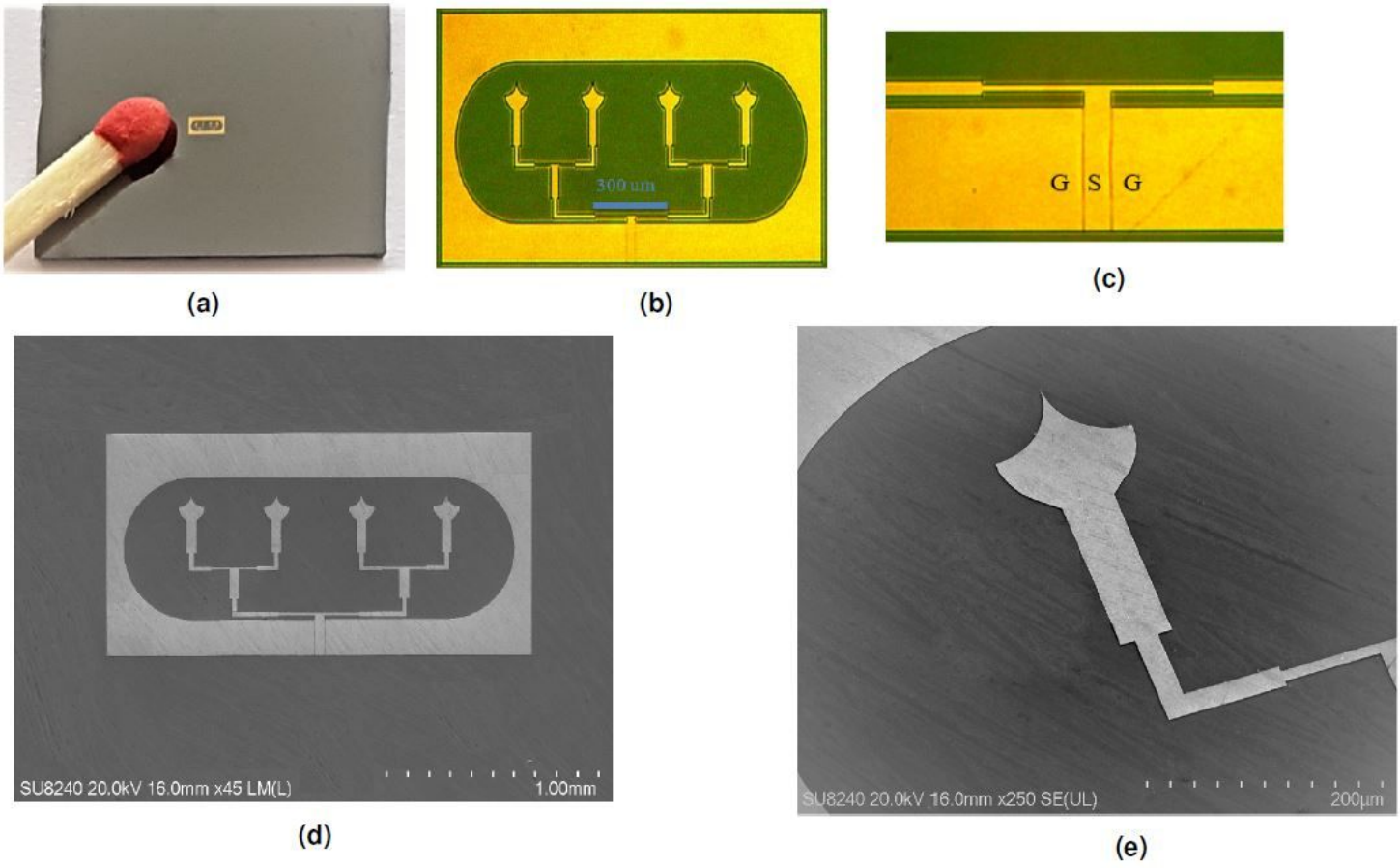

Figure 4

(a) Comparison of the size of the fabricated 1×4 PICA array with a matchstick. Photomicrographs of: (b) the array structure and, (c) the ungrounded CPW feeding network. High-resolution images obtained using a FESEM of: (d) Array structure and, (e) feeding transmission line for a PICA element of the array.

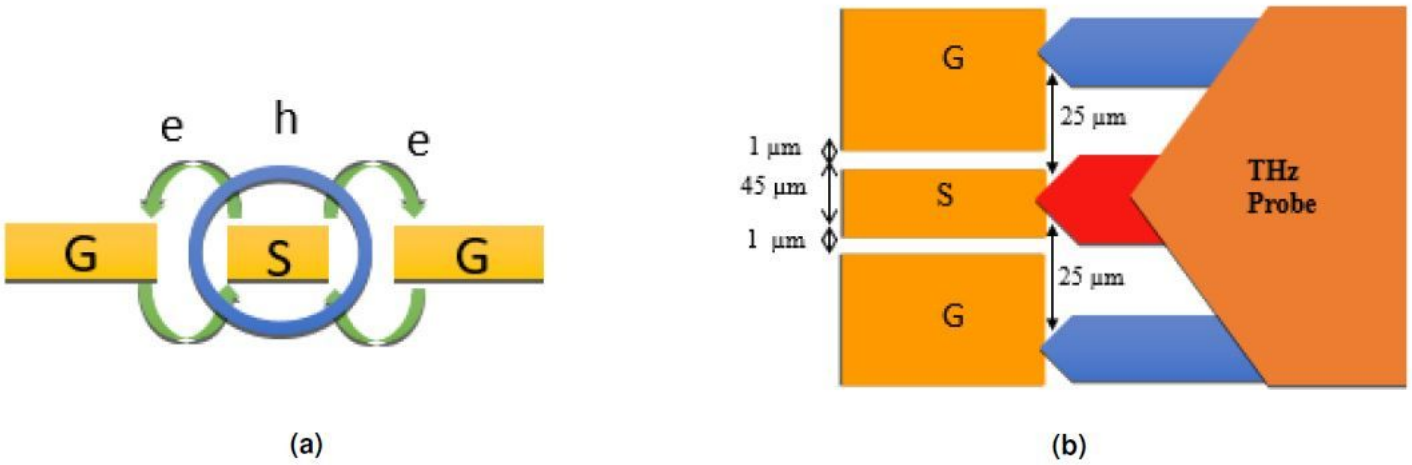

Figure 5

The ungrounded CPW feeding network. (a) Illustration of the electric and magnetic field distributions around the ungrounded CPW and, (b) schematic of the probe measurement contact with the central signal transmission line (S) and ground plane (G).

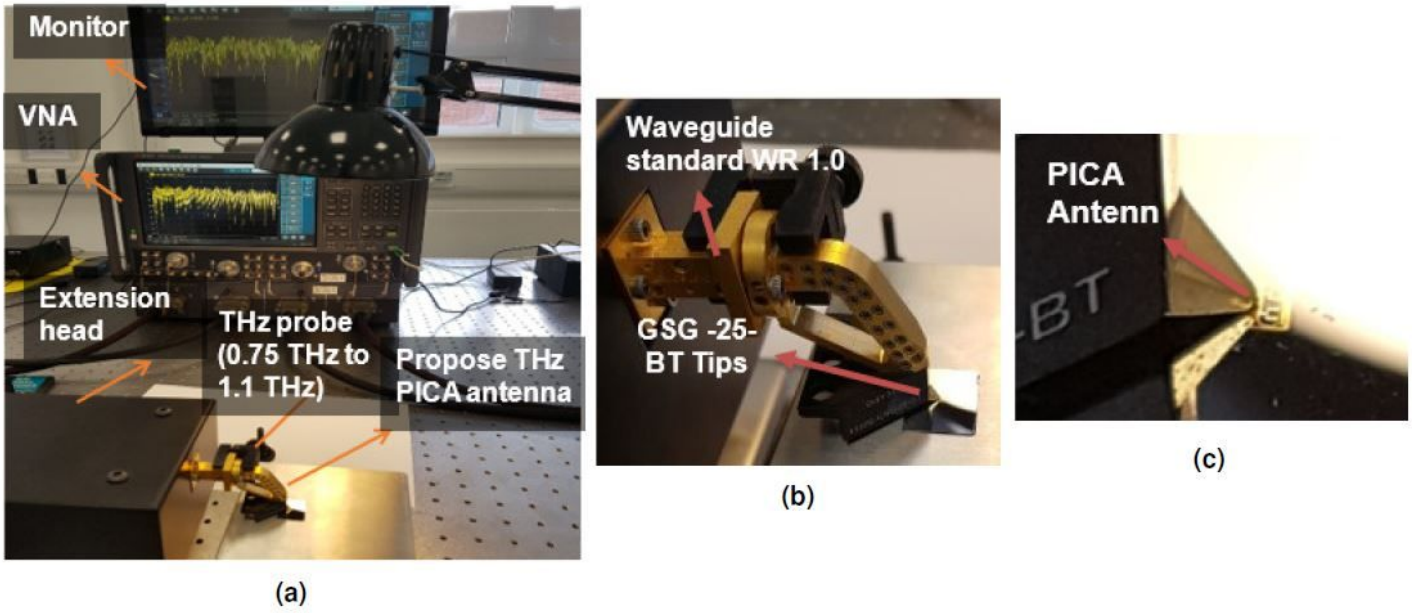

Figure 6

The experimental setup used to measure the scattering parameters. (a) Eye-view of the setup, (b) a GSG-25-BT THz probe (0.75 - 1.10 THz) contact location and, (c) placement of the probe on the PICA.

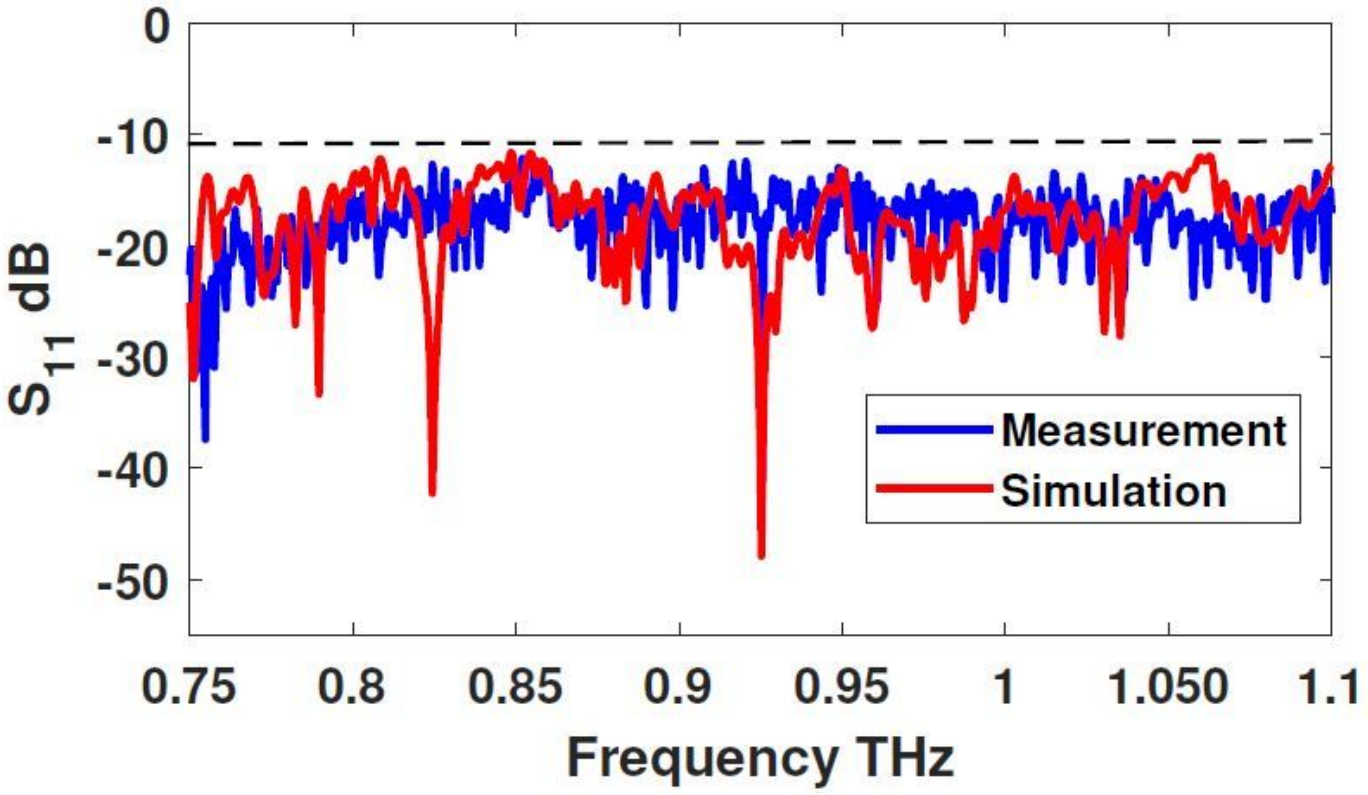

Figure 7

Measured and simulated reflection coefficient of the 1 x 4 PICA array array.

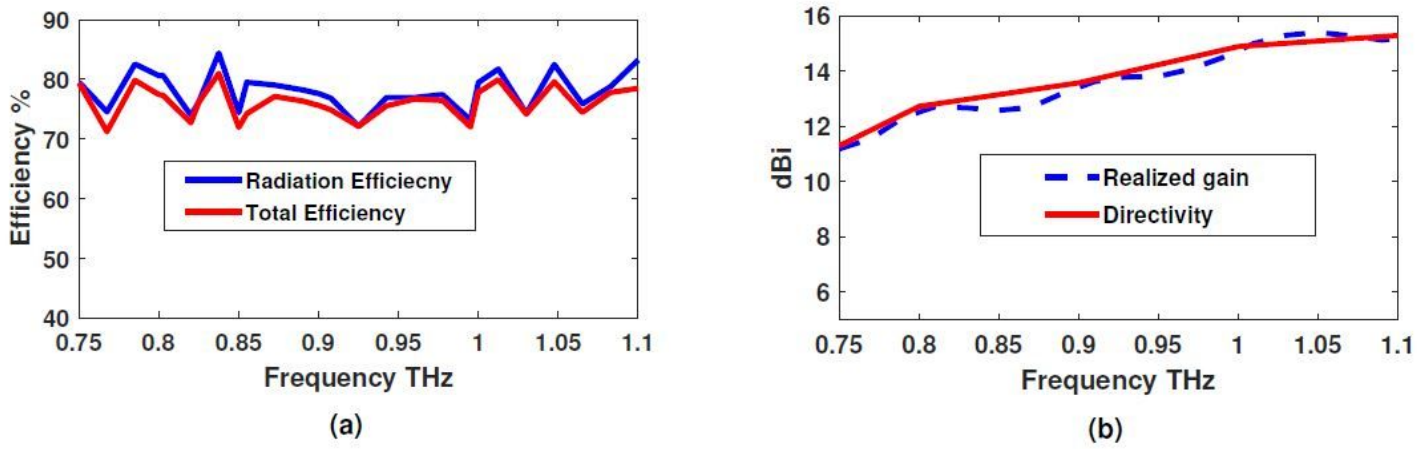

Figure 8

Simulated results of the 1 x 4 PICA array, where (a) the radiation and total efficiency is shown and in, (b) the realised gain.

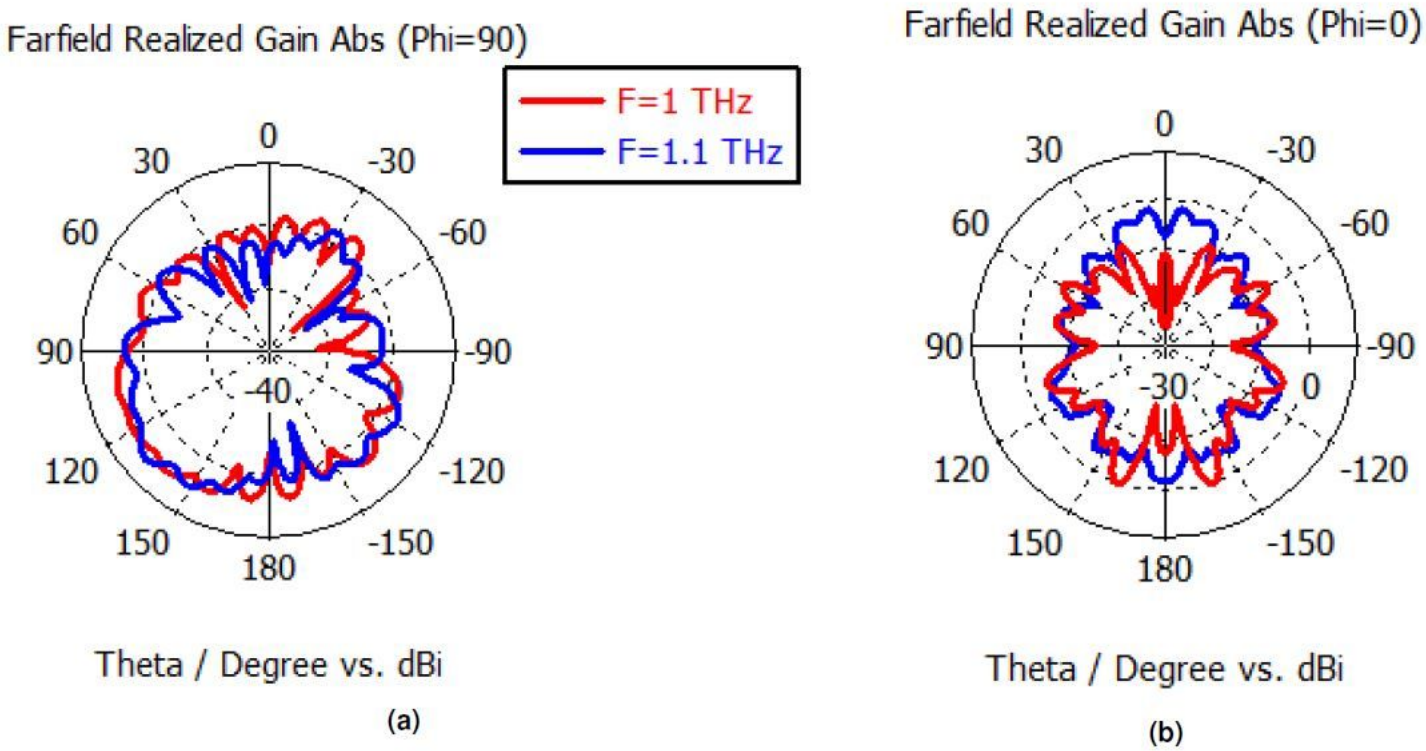

Figure 9

Simulated radiation pattern of the proposed antenna element at different frequencies throughout the operating band. f = 1.0 THz, and f = 1.10 THz

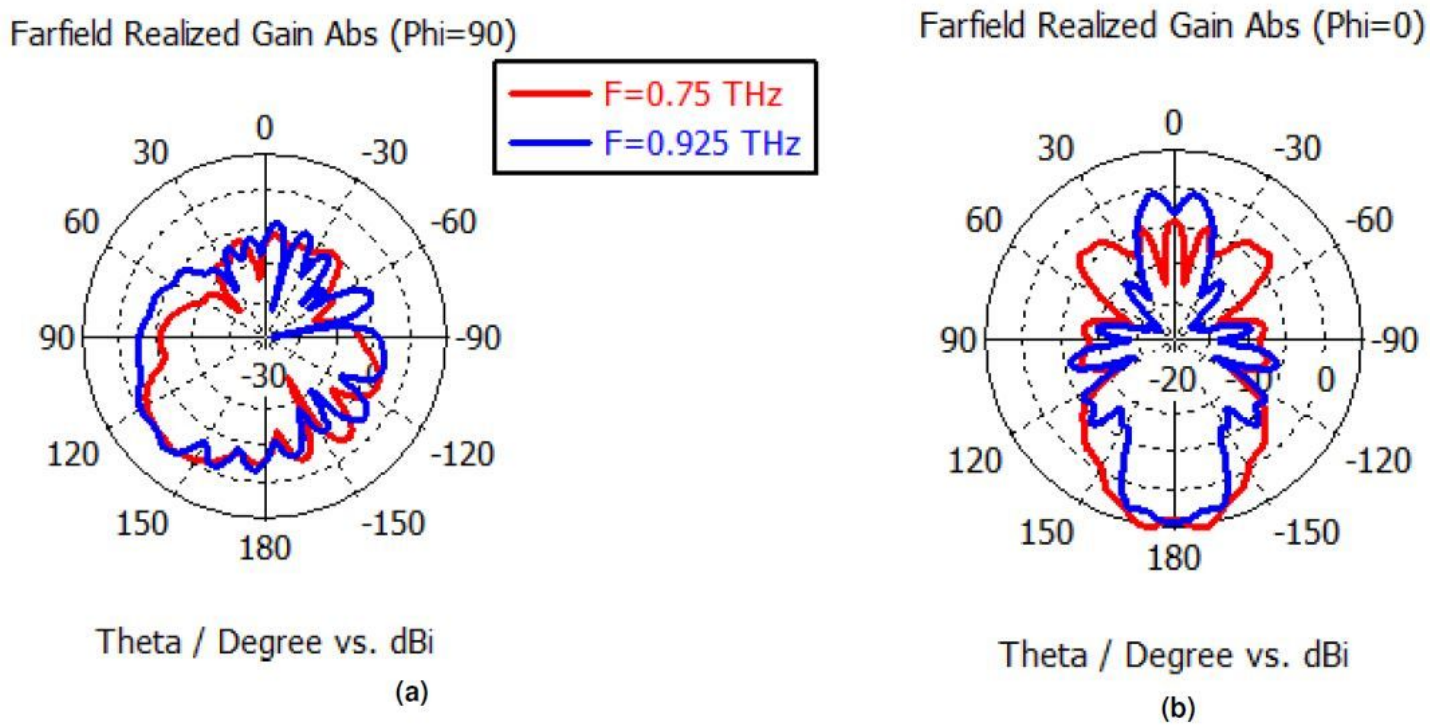

Figure 10

Simulated radiation pattern of the proposed antenna element at two frequencies, 0.75 THz, and 0.925 THz.